# Imaging overturning reflections by Riemannian Wavefield Extrapolation [a]

[a]Published in Journal of Seismic Exploration, 15, no 3, 209-223 (2006)

**Paul Sava**

**(Colorado School of Mines)**

(August 29, 2013)

Running head:

## ABSTRACT

Correctly propagating waves from overhanging reflectors is crucial for imaging in complex geology. This type of reflections are difficult or impossible to use in imaging using one-way downward continuation, because they violate an intrinsic assumption of this imaging method, i.e. vertical upward propagation of reflection data.

Riemannian wavefield extrapolation is one of the techniques developed to address the limitations of one-way wavefield extrapolation in Cartesian coordinates. This method generalizes one-way wavefield extrapolation to general Riemannian coordinate system. Such coordinate systems can be constructed in different ways, one possibility being construction using ray tracing in a smooth velocity model from a starting plane in the imaged volume. This approach incorporates partially the propagation path into the coordinate system and leaves the balance for the one-way wavefield extrapolation operator. Thus, wavefield extrapolation follows overturning wave paths and extrapolated waves using low-order operators, which makes the extrapolation operation fast and robust.

# INTRODUCTION

Imaging of steeply-dipping reflectors, e.g. faults or salt flanks, is a crucial step in seismic imaging of complex geology. In particular, accurate positioning of overhanging salt-flanks influences the quality of migrated images in subsalt regions which are increasingly regarded as the most important targets for seismic exploration.

This challenge for seismic imaging lead to development of many techniques addressing this problem. Among the developned techniques, we can identify:

- **Kirchhoff migration** techniques based on traveltimes computed from overturning rays (Hill et al., 1991; Gray et al., 2001). Such techniques could be used for imaging of reflections at arbitrary dip angles. However, traveltime computation in complex velocity media requires model approximations, e.g. smoothing of sharp velocity boundaries. Furthermore, Kirchhoff migration using multiple arrivals is possible, but technically challenging.

- **Reverse-time migration**, based on solutions of the acoustic wave-equation, also has the potential to image reflectors at arbitrary dip angles. Furthermore, such techniques allow for imaging of multiply-reflected waves. However, reverse-time migration is computationally expensive, which limits its usability in practical imaging problems. Nevertheless, despite its large computational cost, reverse-time migration is gaining popularity.

- **Wavefield extrapolation migration** is also employed in imaging steeply dipping reflectors, despite the intrinsic dip limitation of typical downward continuation operators. However, these techniques have been modified in various ways to allow for imaging of overturning energy. For example, Hale et al. (1992) and Zhang et al. (2006) employ a succession of downward/upward continuation; Rietveld and Berkhout (1994) and Shan and Biondi (2004)

use tilted coordinates to bring the direction of extrapolation closer to the direction of wave propagation; Brandsberg-Dahl and Etgen (2003) use extrapolation along beams to achieve even tighter proximity of the directions of extrapolation and wave propagation; Sava and Fomel (2005) use one-way extrapolation in general (Riemannian) coordinate systems.

This paper concentrates on using Riemannian wavefield extrapolation (RWE) for imaging reflectors with high dip angles. The basic characteristics of RWE recommend it as a good candidate for imaging of steeply-dipping reflectors: like a Kirchhoff technique, the (overturning) Riemannian coordinate system allows extrapolation of waves along their natural direction of propagation; like a wavefield extrapolation technique, RWE allows for extrapolation of all branches of the wavefield, thus making used of all multiple-paths of extrapolated wavefields. Extrapolation in Cartesian coordinates, including tilted coordinates, and extrapolation along beams, represent special cases of RWE for particular choices of the coordinate system. Coordinate systems for RWE can be constructed by ray tracing or by other approaches based on alternative criteria, e.g. conformal maps with topography (Shragge and Sava, 2005).

This paper demonstrates the applicability of RWE to the problem of imaging steeply-dipping reflectors, in particular (overhanging) salt flanks. In addition to accurate implementation of extrapolation, a challenge for RWE is represented by the construction of the coordinate system that is appropriate for imaging of particular reflectors. Thus, a large fraction of this paper is dedicated to coordinate-system construction methods.

This paper is organized as follows: we begin with a brief review of Riemannian wavefield extrpaolation, then describe alternatives for the construction of coordinate systems supporting RWE, and demonstrate the technique with applications to imaging of overhanging salt flank for synthetic salt modeled data.

## RIEMANNIAN WAVEFIELD EXTRAPOLATION

Riemannian wavefield extrapolation (Sava and Fomel, 2005) generalizes solutions to the Helmholtz equation of the acoustic wave-equation

$$\Delta \mathcal{U} = -\omega^2 s^2 \mathcal{U} \,, \tag{1}$$

to non-Cartesian coordinate systems, such that extrapolation is not performed strictly in the downward direction. In equation 1, $s$ is slowness, $\omega$ is temporal frequency, and $\mathcal{U}$ is a monochromatic acoustic wave.

Assume that we describe the physical space in Cartesian coordinates $x$, $y$ and $z$, and that we describe a Riemannian coordinate system using coordinates $\xi$, $\eta$ and $\zeta$ related through a generic mapping

$$x = x(\xi,\eta,\zeta) \,, \tag{2}$$

$$y = y(\xi,\eta,\zeta) \,, \tag{3}$$

$$z = z(\xi,\eta,\zeta) \,, \tag{4}$$

which allows us to compute derivatives of the Cartesian coordinates relative to the Riemannian coordinates.

Following the derivation of Sava and Fomel (2005), the acoustic wave-equation in Riemannian coordinates can be written as:

$$c_{\zeta\zeta}\frac{\partial^2 \mathcal{U}}{\partial \zeta^2} + c_{\xi\xi}\frac{\partial^2 \mathcal{U}}{\partial \xi^2} + c_{\eta\eta}\frac{\partial^2 \mathcal{U}}{\partial \eta^2} + c_{\xi\eta}\frac{\partial^2 \mathcal{U}}{\partial \xi \partial \eta} = -\left(\omega s\right)^2 \mathcal{U} \,. \tag{5}$$

where coefficients $c_{ij}$ are spatially-variable functions of the coordinate system and can be computed numerically for any given coordinate system using the mappings 2-4.

The acoustic wave-equation in Riemannian coordinates 5 ignores the influence of first order

terms present in a more general acoustic wave-equation in Riemannian coordinates. This approximation is justified by the fact that, according to the theory of characteristics for second-order hyperbolic equations (Courant and Hilbert, 1989), the first-order terms affect only the amplitude of the propagating waves.

From equation 5 we can derive a dispersion relation of the acoustic wave-equation in Riemannian coordinates

$$-c_{\zeta\zeta}k_\zeta^2 - c_{\xi\xi}k_\xi^2 - c_{\eta\eta}k_\eta^2 - c_{\xi\eta}k_\xi k_\eta = -\left(\omega s\right)^2 \ , \tag{6}$$

where $k_\zeta$, $k_\xi$ and $k_\eta$ are wavenumbers associated with the Riemannian coordinates $\zeta$, $\xi$ and $\eta$. For one-way wavefield extrapolation, we need to solve the quadratic equation 6 for the wavenumber of the extrapolation direction $k_\zeta$, and select the solution with the appropriate sign for the desired extrapolation direction:

$$k_\zeta = \sqrt{\frac{\left(\omega s\right)^2}{c_{\zeta\zeta}} - \frac{c_{\xi\xi}}{c_{\zeta\zeta}}k_\xi^2 - \frac{c_{\eta\eta}}{c_{\zeta\zeta}}k_\eta^2 - \frac{c_{\xi\eta}}{c_{\zeta\zeta}}k_\xi k_\eta} \ . \tag{7}$$

The coordinate system coefficients $c_{ij}$ and the extrapolation slowness $s$ can be combined to form a reduced set of parameters. In 2D, for example, all coordinate-system coefficients can be represented by 2 parameters, $a$ and $b$. Further extensions and implementation details of equation 7 are described by Sava and Fomel (2007).

Extrapolation using equation 7 implies that the coefficients defining the medium and coordinate system are not changing spatially. In this case, we ca perform extrapolation using a simple phase-shift operation

$$\mathcal{U}_{\tau+\Delta\tau} = \mathcal{U}_\tau e^{ik_\tau \Delta\tau} \ , \tag{8}$$

where $\mathcal{U}_{\tau+\Delta\tau}$ and $\mathcal{U}_\tau$ represent the acoustic wavefield at two successive extrapolation steps, and $k_\tau$ is the extrapolation wavenumber defined by equation 7.

For media with variability of the coefficients $c_{ij}$ due to either velocity variation or focusing/defocusing of the coordinate system, we cannot use in extrapolation the wavenumber computed directly using equation 7. Like for the case of extrapolation in Cartesian coordinates, we can approximate the wavenumber $k_\tau$ using series expansions relative to coefficients $c_{ij}$ present in the dispersion relation 7. Such approximations can be implemented in the space-domain, in the Fourier domain or in mixed space-Fourier domains (Sava and Fomel, 2007).

## COORDINATE SYSTEMS

Riemannian wavefield extrapolation operates in coordinate systems that may or may not be defined according to the model used for imaging. As indicated earlier, there are several options for constructing such coordinate systems, but the solution selected for the case described in this paper uses ray tracing. In this case, the coordinate system is semi-orthogonal, i.e. the extrapolation direction is orthogonal to the other two directions defining a 3D coordinate system. Cartesian coordinates are special cases of Riemannian coordinates constructed by tracing rays orthogonal to a flat surface in constant velocity.

The accuracy of one-way wavefield extrapolation operators maximizes in the direction of extrapolation (vertical for downward continuation; along rays for Riemannian coordinate systems constructed by ray tracing). In addition, for steeply dipping reflectors, the angle of reflection is likely to be relatively small since this reflector is illuminated from a large distance using a small limite acquisition aperture.

It is thus desirable to construct a coordinate system that minimizes the angles between the extrapolation direction, and the directions of wave propagation and normal to the imaged reflectors. One way to achieve this goal is to construct the coordinate system by tracing rays orthogonal to an

imaginary line (plane in 3D) located behind the overhanging reflector.

These ideas are illustrated with a model based on the Sigsbee 2A synthetic (Paffenholz et al., 2002) extended vertically and horizontally to allow diving waves from the overhanging salt flank to arrive at the surface. Figure 1a shows an example of Riemannian coordinates constructed from ray tracing from behind the salt flank reflector. For comparison, Figure 1b shows a Cartesian coordinate system tilted relative to the vertical direction to minimize the angle between the extrapolation direction and the normal to the reflector.

As indicated in the preceding section, we can describe Riemannian coordinate systems with several coefficients incorporating all the information about the coordinate system shape and the extrapolation slowness. For this 2D example, there are two coefficients, $a$ and $b$ depicted in Figures 2a-2b for the Riemannian coordinate system and in Figures 3a-3b for the tilted Cartesian coordinate system. The plots depict $a$ and $b$ function of the Riemannian coordinates, $\tau$ and $\gamma$. $\tau$ has time units and it represents the extrapolation direction, and $\gamma$ is non-dimensional and represents an index of the rays shot from the linear origin behind the imaged reflector.

Coefficient $a$ describes the ratio of the extrapolation velocity to the velocity used for ray tracing, and coefficient $b$ describes the focusing/defocusing of the coordinate system. In both cases, coefficient $a \neq 1$ since the velocity used for extrapolation is different from the velocity used for the coordinate system. For the Cartesian coordinate system, coefficient $b$ is a constant, as depicted in Figure 3b.

Figures 2c and 3c depict the acquisition surface and the salt body outline mapped in Riemannian and tilted Cartesian coordinates, respectively. We can observe that in Riemannian coordinates, the overhanging salt flank is nearly orthogonal to the extrapolation direction, unlike its layout in tilted Cartesian coordinates. Therefore, imaging accuracy for such reflectors can be achieved in

Riemannian coordinates with lower order extrapolation kernels than in the case of tilted Cartesian coordinates, as demonstrated in the following section.

## EXAMPLE

The Riemannian wavefield extrapolation imaging procedure is illustrated with the synthetic example introduced in the preceding section. Exploding reflector data are modeled from all edges of the salt body and recorded at all locations along the surface. The data are modeled using time-domain finite-differences. No attempt is made to suppress the multiples, thus some of them are present in the migrated images.

Figures 4a-4b depict wavefields at 5 and 10 seconds from the exploding reflector moment, respectively. As expected, the wavefield originating on the overhanging salt flank dives and then returns to the surface (Figure 5). Other parts of the wavefield either propagate straight up to the surface, or propagate away from it and are not recorded. The imaged components of the recorded wavefield are those overturning to the surface at locations intersected by the coordinate system.

The overturned data collected at the surface are imaged in Riemannian and tilted Cartesian coordinates using the systems depicted in Figures 1a-1b, characterized by coefficients $a$ and $b$ depicted in Figures 2a-2b and Figures 3a-3b, respectively.

Figures 6a-6b show the migrated image obtained by wavefield extrapolation in Riemannian coordinates. Panel 6a depicts the image in the Riemannian space, and panel 6b depicts the same image after mapping to vertical Cartesian coordinates. Both overhanging reflectors, on opposite sides of the salt body, are imaged correctly demonstrating successful imaging with overturning waves in Riemannian coordinates.

Figures 7a-7b show analogous images obtained by extrapolation in tilted Cartesian coordinates.

Imaging is performed using the same extrapolation as the one used for imaging in Riemannian coordinates. The only difference is the coordinate system, therefore all image differences are caused strictly by the coordinate system and not by the extrapolation or imaging operators.

Unlike for the preceding example, the overhanging salt flanks are not positioned correctly, as seen by comparing Figures 6a and 7a. The reason for the inaccurate reflector positioning is the limited accuracy of the extrapolation operator at high angles relative to the extrapolation direction. While the Riemannian coordinate system has the flexibility to minimize the angle between the extrapolation direction and the direction of wave propagation, the tilted Cartesian coordinate system cannot do that, thus requiring wavefield extrapolation at high angles. In this example, modifying the tilt angle of the Cartesian coordinate system does not help since propagation at high angles occurs both in the vicinity of the reflector and close to the acquisition surface. Furthermore, the Riemannian coordinate system represents the natural direction of wave propagation, unlike the tilted Cartesian coordinate system which is artificial and has no physical relation to the propagating waves.

## CONCLUSIONS

This paper demonstrates the applicability of Riemannian wavefield extrapolation to the problem of imaging overhanging salt flanks. Imaging such reflectors using one-way wavefield extrapolation in Cartesian coordinates is impractical since waves propagate partially down, partially up. A possible solution to this problem consists of using tilted Cartesian coordinate systems. This procedure partially reduces the angle between the direction of wave propagation and the direction of extrapolation. However, even in this coordinate framework, waves need to be extrapolated at high angles up to $90^\circ$ which degrades the imaging accuracy.

In contrast, wavefield extrapolation in Riemannian coordinates has the flexibility to follow

closely the paths of wave propagation. Therefore, the relative angle between the direction of extrapolation and the direction of wave propagation is much smaller than in the case of extrapolation in tilted Cartesian coordinates, thus improving imaging accuracy.

Overturning reflections can, in principle, be imaged using Kirchhoff migration. However, this imaging procedure has difficulty producing accurate images in complex geology characterized by wave multipathing and sharp velocity variation. In contrast, imaging overturning reflections using Riemannian wavefield extrapolation benefits from all characteristics of one-way wavefield extrapolation, i.e. stability accross boundaries between media with large velocity variation, multipathing, etc.

## ACKNOWLEDGMENT

ExxonMobil provided partial financial support of this research.

## REFERENCES


Brandsberg-Dahl, S., and J. Etgen, 2003, Beam-wave imaging: 73rd Ann. Internat. Mtg., Soc. of Expl. Geophys., 977–980.

Courant, R., and D. Hilbert, 1989, Methods of mathematical physics: John Wiley & Sons.

Gray, S. H., J. Etgen, J. Dellinger, and D. Whitmore, 2001, Seismic migration problems and solutions: Geophysics, **66**, 1622–1640.

Hale, D., N. R. Hill, and J. Stefani, 1992, Imaging salt with turning seismic waves: Geophysics, **57**, 1453–1462. (Discussion and reply by authors in GEO-58-8-1205-1206).

Hill, N. R., T. H. Watson, M. H. Hassler, and K. L. Sisemore, 1991, Salt-flank imaging using Gaussian beam migration: 61st Ann. Internat. Mtg, Soc. of Expl. Geophys., 1178–1180.

Paffenholz, J., B. McLain, J. Zaske, and P. Keliher, 2002, Subsalt multiple attenuation and imaging: Observations from the Sigsbee2B synthetic dataset: 72nd Annual International Meeting, SEG, Soc. of Expl. Geophys., 2122–2125.

Rietveld, W. E. A., and A. J. Berkhout, 1994, Prestack depth migration by means of controlled illumination: Geophysics, **59**, 801–809.

Sava, P., and S. Fomel, 2005, Seismic imaging using Riemannian wavefield extrapolation: Geophysics, **70**, T45–T56.

———, 2007, High-order kernels for Riemannian wavefield extrapolation: Geophysical Prospecting, **56**, 49–60.

Shan, G., and B. Biondi, 2004, Imaging overturned waves by plane-wave migration in tilted coordinates: 74th Ann. Internat. Mtg., Soc. of Expl. Geophys., 969–972.

Shragge, J., and P. Sava, 2005, Wave-equation migration from topography: 75th Ann. Internat. Mtg., Expanded Abstracts, Soc. of Expl. Geophys., 1842–1845.

Zhang, Y., S. Xu, and G. Zhang, 2006, Imaging complex salt bodies with turning-wave one-way

wave equation migration: Presented at the 68th Mtg., Abstracts, Eur. Assoc. Expl. Geophys.

## LIST OF FIGURES

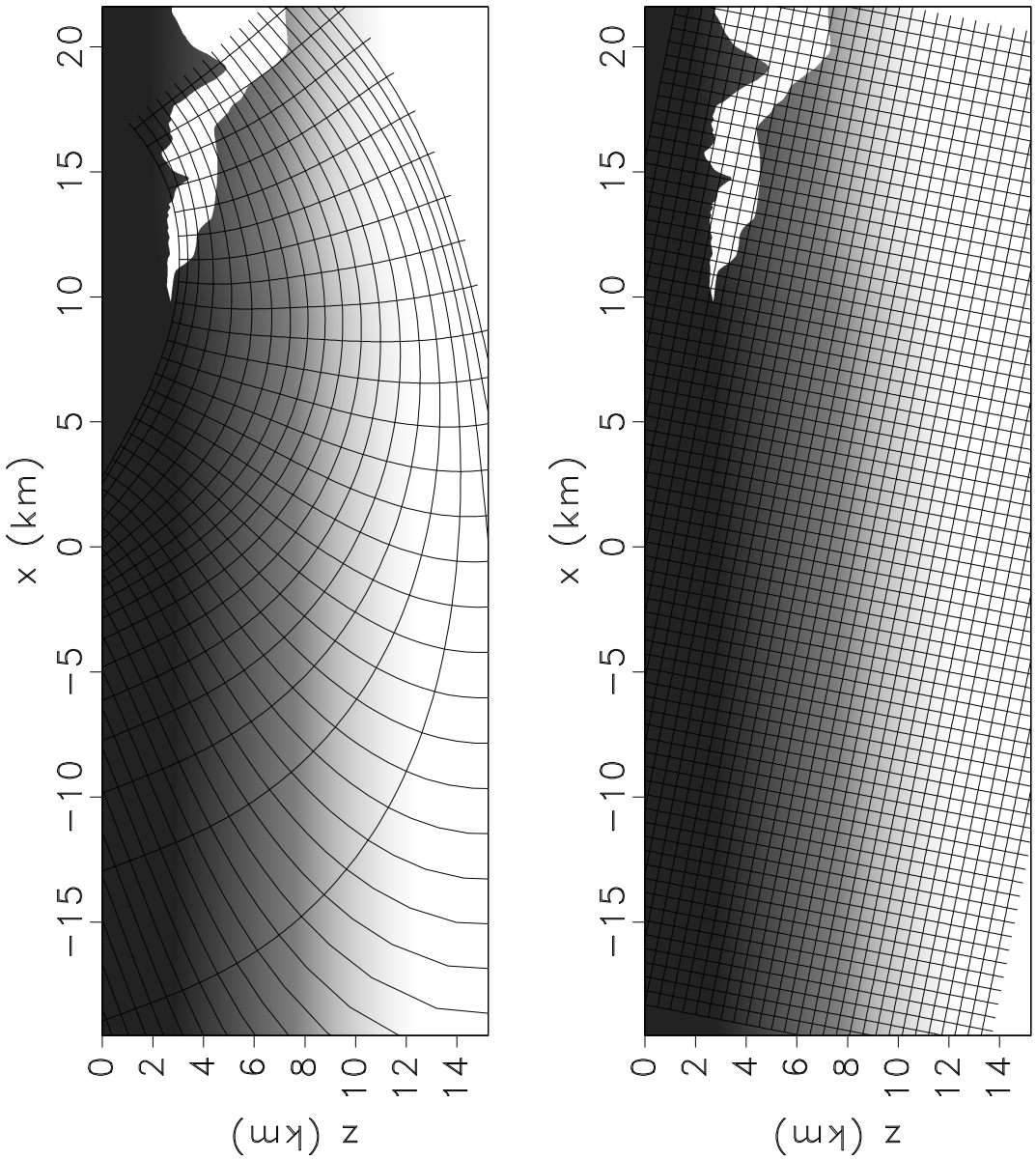


Figure 1: Riemannian coordinate system (a) and tilted Cartesian coordinate system (b). –

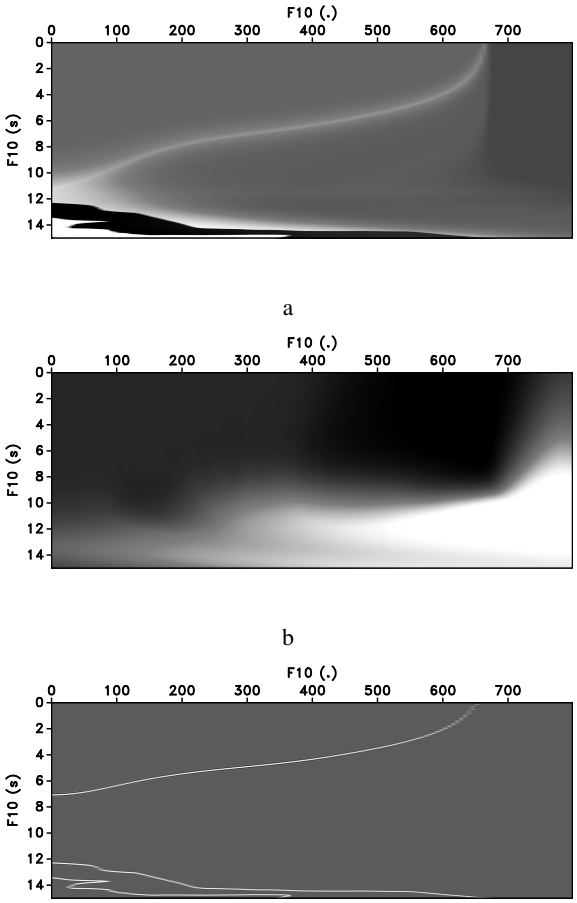


Figure 2: Riemannian coordinate system coefficients, (a) and (b), and outline of acquisition geometry and salt body (c).

–

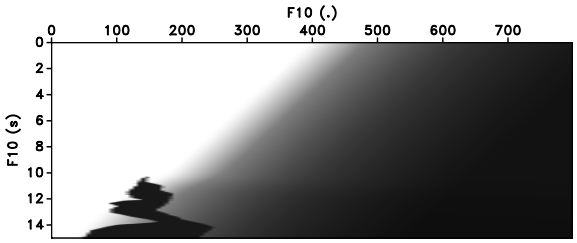


a

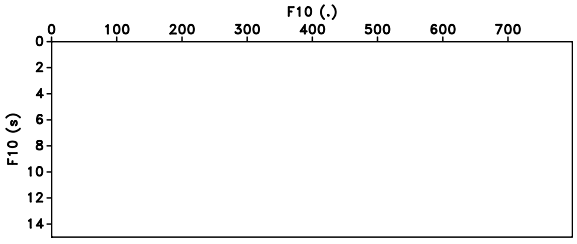


b

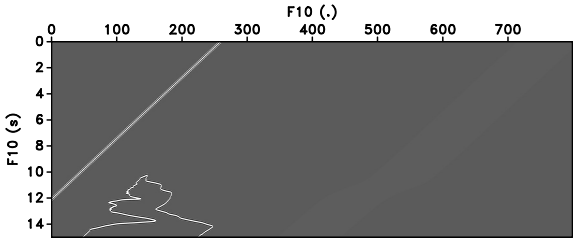


c

Figure 3: Tilted Cartesian coordinate system coefficients, (a) and (b), and outline of acquisition geometry and salt body (c).

–

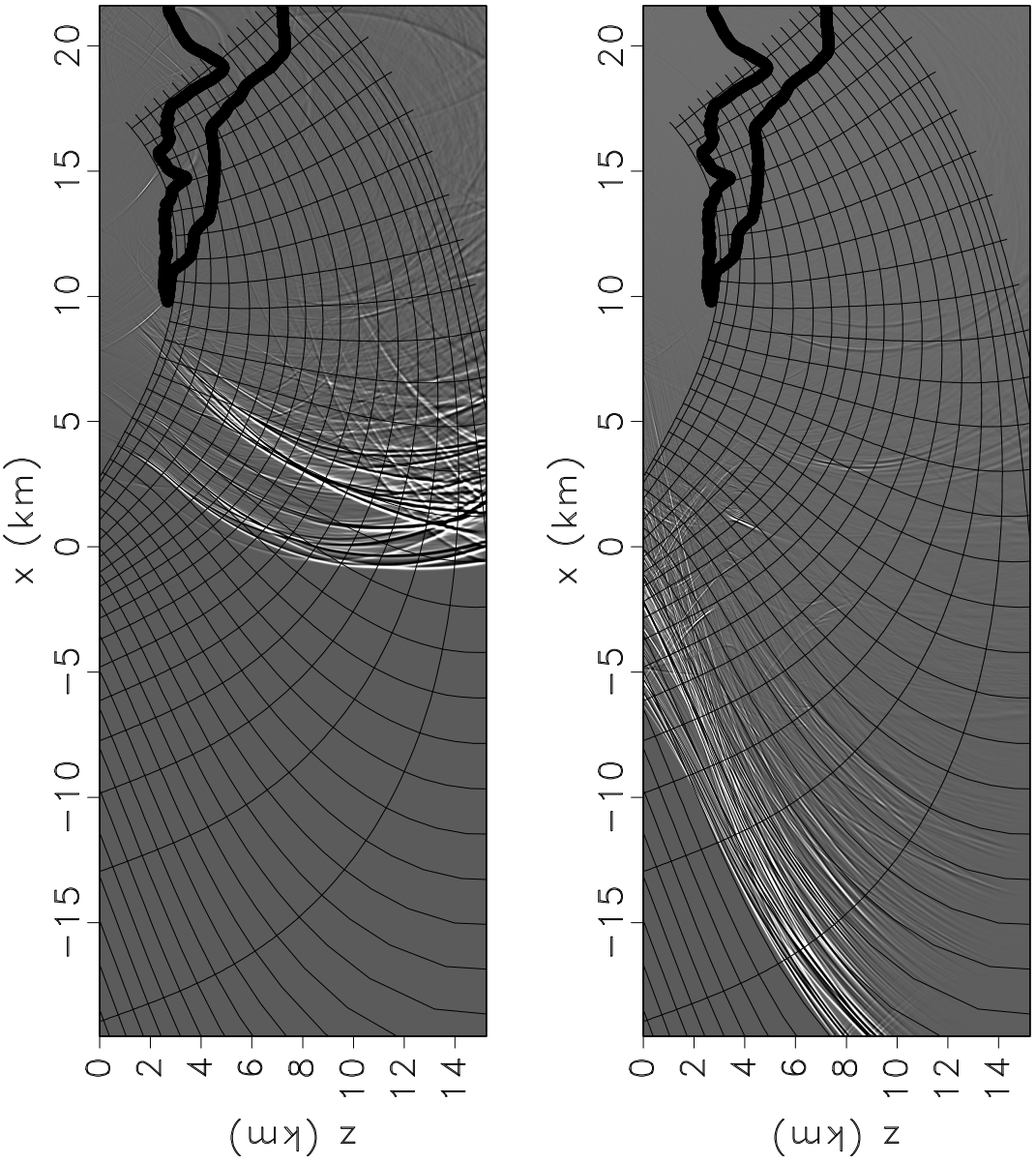


Figure 4: Wavefield from the overhanging salt flank at $t = 5, 10$ s from the moment of exploding reflectors on the salt body.

–

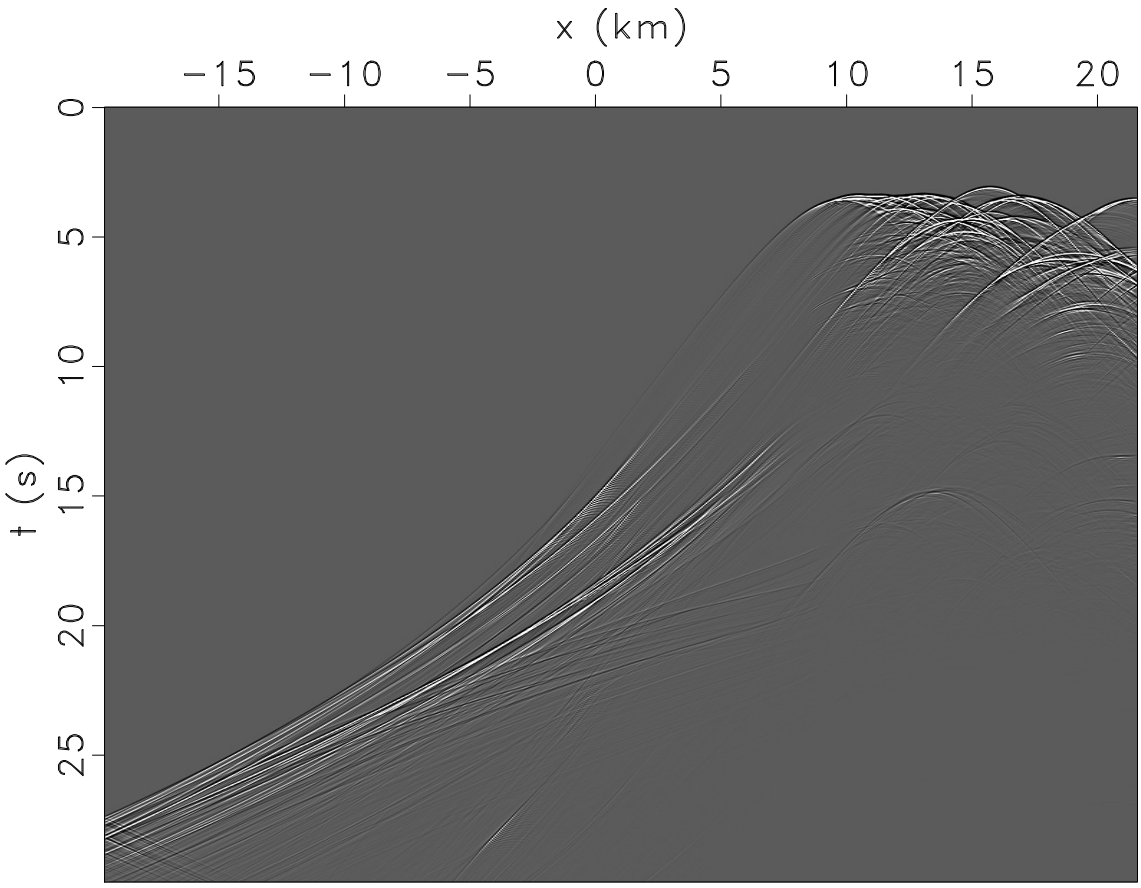


Figure 5: Recorded data at the surface. Overturning energy is recorded from $x = -20$ km to $x = 0$ km at $t = 15 - 25$ s.

–

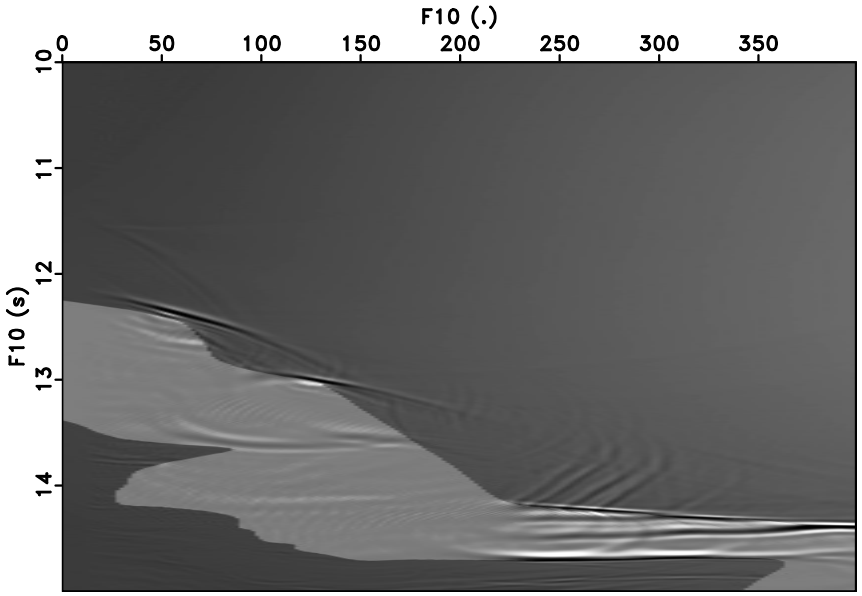


a

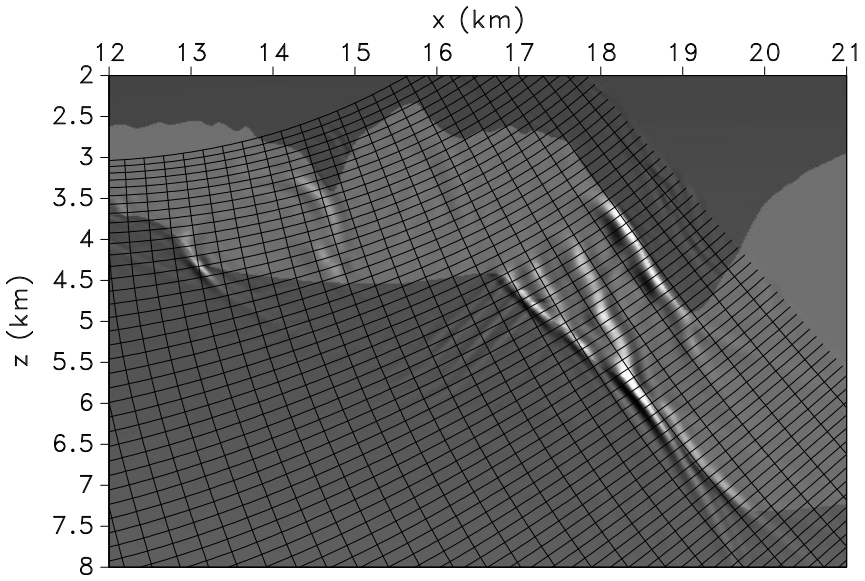


b

Figure 6: Migrated images using wavefield extrapolation in Riemannian coordinates with a Fourier finite-differences (F15) kernel. Panel (a) depicts the image in Riemannian coordinates, and panel (b) depicts the same image mapped to vertical Cartesian coordinates.

–

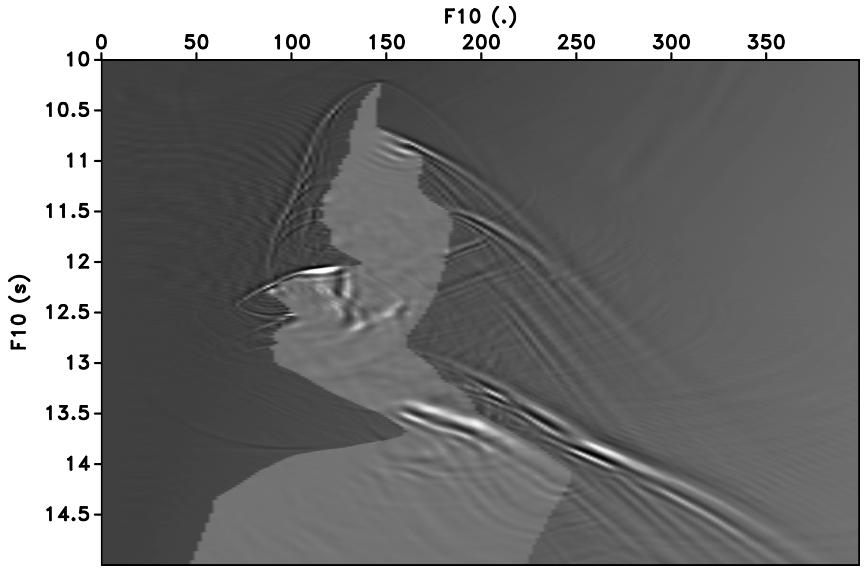


a

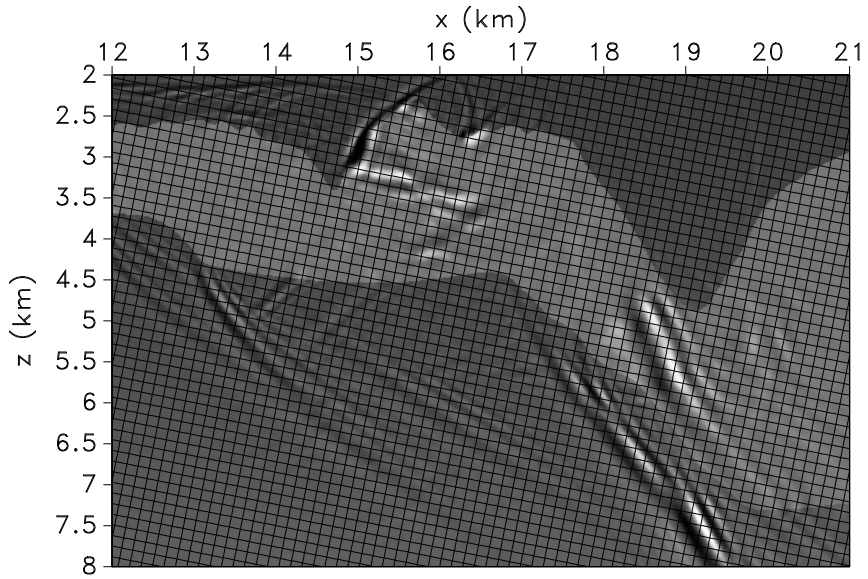


b

Figure 7: Migrated images using wavefield extrapolation in tilted Cartesian coordinates with a Fourier finite-differences (F15) kernel. Panel (a) depicts the image in tilted Cartesian coordinates, and panel (b) depicts the same image mapped to vertical Cartesian coordinates.

–